Ultrasound in Med. & Biol., Vol. 35, No. 10, pp. 1647–1661, 2009

0301-5629/09/$–see front matter

ELSEVIER

doi:10.1016/j.ultrasmedbio.2009.05.004

● *Original Contribution*

INSTANTANEOUS FREQUENCY-BASED ULTRASONIC TEMPERATURE ESTIMATION DURING FOCUSED ULTRASOUND THERMAL THERAPY

Hao-Li Liu,* Meng-Lin Li,† Tzu-Ching Shih,‡ Sheng-Min Huang,* I-Yeh Lu,* Deng-Yn Lin,§ Shi-Ming Lin,§ and Kuen-Cheng Ju¶

*Department of Electrical Engineering and Biomedical Engineering Center, Chang-Gung University, Taoyuan; †Department of Electrical Engineering, National Tsing-Hua University, Hsinchu; ‡Institute of Medical Radiology Technology, China Medical University, Taichung; §Department of Internal Medicine, Chang-Gung Memorial Hospital, Taoyuan; and ¶Department of Biomedical Engineering, I-Shou University, Kaohsiung, Taiwan

(*Received* 25 *March* 2008; *revised* 29 *April* 2009; *in final form* 11 *May* 2009)

Abstract—Focused ultrasound thermal therapy relies on temperature monitoring for treatment guidance and assurance of targeting and dose control. One potential approach is to monitor temperature change through ultrasonic-backscattered signal processing. The current approach involves the detection of echo time-shifts based on cross-correlation processing from segmented radiofrequency (RF) data. In this study, we propose a novel ultrasonic temperature-measurement approach that detects changes in instantaneous frequency along the imaging beam direction. Focused ultrasound was used as the heating source, and the 1-D beamformed RF signals provided from an ultrasound imager were used to verify the proposed algorithm for temperature change estimation. For comparison, a conventional cross-correlation technique was also evaluated. Heating experiments testing tissue-mimicking phantoms and *ex vivo* porcine muscles were conducted. The results showed that temperature can be well estimated by the proposed algorithm in the temperature range, where the relationship of sound speed *versus* temperature is linear. Compared with the cross-correlation–based algorithm, the proposed new algorithm yields a six-fold increase in computational efficiency, along with comparable contrast-detection ability and precision. This new algorithm may serve as an alternative method for implementing temperature estimation into a clinical ultrasound imager for thermal therapy guidance. (E-mail: kcju@isu.edu.tw) © **2009 World Federation for Ultrasound in Medicine & Biology.**

Key Words: **Ultrasound temperature estimation, Focused ultrasound, Instantaneous frequency, Zero crossing.**

INTRODUCTION

High-intensity focused ultrasound (HIFU) technology was introduced half a century ago, and it has proven to be capable of noninvasively delivering concentrated energy to positions located deep within the human body to induce localized thermal coagulation (Lynn et al. 1942; ter Haar 1995). The technology has also been recently used in clinical treatments (Tempany et al. 2003; Wu et al. 2004; Rabinovici et al. 2007; Stewart et al. 2007; ter Haar and Coussios 2007). During HIFU treatments, temperature monitoring for treatment guidance is essential to quantify thermal dosage for better treatment control. Among current medical imaging modalities, magnetic resonance imaging (MRI) has been proven to detect temperature changes precisely during treatment because of the effect of temperature-dependent proton resonance frequency shifts (Lynn et al. 1942; ter Haar 1995; Tempany et al. 2003). However, to use MRI for temperature monitoring, the HIFU system must be designed to be compatible with magnetic resonance, which largely increases the complexity of the system design and increases the cost for its use in clinical applications. Diagnostic ultrasound is another potential approach that provides sufficient temperature sensitivity and yields good spatial resolution for medical imaging. The basic concept of this approach is that the backscattered ultrasound RF echo from the region experiences time shifts after the tissue is heated; this phenomenon has been identified to be a gross effect that includes the change in the sound speed and thermal expansion of the tissue in the heated region due to temperature changes (Nasoni and Bowen 1989). An attractive feature of using diagnostic ultrasound to monitor temperature during HIFU

Address correspondence to: Kuen-Cheng Ju, Ph.D., Department of Biomedical Engineering, I-Shou University, Kaohsiung, Taiwan. E-mail: kcju@isu.edu.tw

treatments is that this technique is relatively inexpensive, portable and can be easily employed in almost any current HIFU system with little concern about system compatibility.

Among the ultrasound-based temperature estimation techniques, both frequency-domain–based and time-domain–based processing schemes have been proposed. Seip et al. (1995) used a spectral processing technique (Nasoni and Bowen 1989). The temperature change estimation along one dimension was achieved by tracking the frequency variation in the echo components in the spectral domain; the echo spectrum was estimated using an autoregressive (AR) model. Compared with spectral-based processing schemes, a major advantage of time-domain processing is its computational efficiency. Maass-Moreno and colleagues proposed that time-domain signal processing schemes such as cross-correlation estimators are feasible for temperature estimation (Maass-Moreno and Damianou 1996; Maass-Moreno et al. 1996). Although the computational efficiency is improved, the cross-correlation computation that has been used previously still involves extensive processing, hindering the progress of the real-time implementation of temperature estimation (Maass-Moreno and Damianou 1996; Maass-Moreno et al. 1996; Simon et al. 1998). In addition to the abovementioned technique, Simon et al. (1998) used a lag-1 autocorrelation estimator to perform temperature estimation, which is conceptually identical to blood-flow estimation using pulsed Doppler systems (Kasai and Namekawa 1985; Bonnefous and Pesque 1986). By using classical quadrature demodulation, the phase differences in successive echoes from heated targets are detected, and the phase change in the signal can be estimated and accumulated. As a result, the temperature information can be extracted.

In this study, we propose using a novel time-domain ultrasonic temperature-estimation technique by detecting changes of instantaneous frequency (IF) along the imaging beam direction. IF detection has been successfully implemented in techniques of consecutive 1-D blood flow monitoring, yielding high temporal resolution (Barber et al. 1985; Boashash 1992a, 1992b). Because such techniques rely entirely on simplified signal processing, they are significantly simpler than frequency-domain processing (such as Fourier transform operations) or convolution operations used in time-domain processing. This yields a relatively easier implementation alternative to the temperature-estimation function in current diagnostic ultrasound systems. In this paper, we present the theoretical derivation and numerical implementation of the algorithm. The experimental results obtained with tissue-mimicking phantoms and *ex vivo* porcine muscles demonstrate the proposed technique; its performance is evaluated by comparing it with the cross-correlation–based algorithm in terms of their spatial resolutions, computational efficiencies and contrast-to-noise ratios.

MATERIALS AND METHODS

Echo time-shift estimation model

Assume that c(T, z) represents the distribution of the speed of sound in the tissue as a function of the temperature T and axial depth z, where z = 0 at the surface of the transducer. If the thermal dependence of the speed of sound is considered, the round-trip transit time t(z) of a pulse echo passing through an inhomogeneous tissue with temperature distribution T(z) and being reflected from depth z can be given by (Seip and Ebbini 1995):

$$t(z)=2\int_0^z \frac{d\xi}{c(\xi,T(\xi))}, \tag{1}$$

where T(z) can be decoupled to a base temperature T_0, with a local temperature change $\delta T(z)$ induced by a given heat source:

$$T(z)=T_0+\delta T(z). \tag{2}$$

When temperature-induced thermal expansion is considered as distance shifting, in (1), dξ can be replaced by $(1+\alpha(\xi)\delta T(\xi))d\xi$, where $\alpha(\xi)$ is the linear coefficient of thermal expansion of the medium at axial depth ξ. Then, by rearranging eqns (1) and (2) and partially differentiating the echo time-shift $\delta t(z)$(*i.e.*, the difference between transit time with and without local temperature change) with respect to z, we can have (Simon et al. 1998):

$$\frac{\partial}{\partial z}(\delta t(z))=2\left[\frac{1+\alpha(z)\delta T(z)}{c(z,T(z))}-\frac{1}{c(z,T_0)}\right], \tag{3}$$

where $\delta t(z)=t(z)-t_0(z)$, and $t_0(z)$ is the transit time without local temperature change being considered. Next, the term $c(z,T(z))$ can be replaced as a temperature-dependent one, $c(z,T(z))=c_0(z)(1+\beta(z)\delta T(z))$, where $\beta(z)=\frac{1}{c(z,T_0)}\bullet\frac{\partial c(z,T)}{\partial T}|_{T=T_0}$ is defined as the thermally induced coefficient of sound speed and c_0 is the initial sound speed. Then we can rewrite eqn (3) as follows:

$$\begin{aligned}\frac{\partial}{\partial z}(\delta t(z))&=2\left[\frac{1+\alpha(z)\delta T(z)}{c(z,T_0)(1+\beta(z)\delta T(z))}-\frac{1}{c(z,T_0)}\right]\\&=2\left[\frac{(\alpha(z)-\beta(z))\delta T(z)}{c_0(z)(1+\beta(z)\delta T(z))}\right]\end{aligned}. \tag{4}$$

The term $|\beta(\xi)\delta T(\xi)|$ is assumed to be considerably smaller than unity so that it can be ignored. Equation (4) can then be further simplified, yielding a linear relationship between temperature increase and echo time-shift:

$$\delta T(z)=\frac{C_0(z)}{2}\cdot\left(\frac{1}{\alpha(z)-\beta(z)}\right)\cdot\frac{\partial}{\partial z}\delta t(z). \quad (5)$$

In the following discussion, we correlate echo time-shift $\delta t(z)$with IF under continuous-wave (CW) approximation. The IF at the specific signal depth z can be defined as

$$IF=\frac{1}{2\pi}\frac{d\phi(t)}{dt}=\frac{1}{2\pi}\frac{d\phi(z)}{dz}, \quad (6)$$

where $\phi(t)$ or $\phi(z)$ denotes the received ultrasound signal phase. In addition, the echo time-shift is encoded in the phase difference between signals before and after (or under) heating (denoted as $\phi_1(z)$ and $\phi_2(z)$, respectively), which can be calculated as follows:

$$\delta t(z)=\frac{1}{2\pi f_0}(\phi_2(z)-\phi_1(z)). \quad (7)$$

Differentiating eqn (7) with respect to z transforms this representation in terms of the spatial IF distribution:

$$\delta t(z)=\frac{1}{f_0}\int_0^z(IF_2(\xi)-IF_1(\xi))d\xi. \quad (8)$$

By substituting eqn (8) in eqn (5), we obtain

$$\delta T(z)=\frac{C_0}{2f_0}\cdot\left(\frac{1}{\alpha(z)-\beta(z)}\right)\cdot\frac{\partial}{\partial z}\left(\int_0^z(IF_2(\xi)-IF_1(\xi))d\xi\right), \quad (9)$$

which can be further simplified as

$$\delta T(z)=\frac{C_0}{2f_0}\cdot\left(\frac{1}{\alpha(z)-\beta(z)}\right)\cdot(IF_2(z)-IF_1(z)). \quad (10)$$

Note that the term $C_0/2f_0\cdot(1/(\alpha(z)-\beta(z)))$ is considered to be consistent based on the assumptions that tissue is subject to the linear range of temperature *versus* sound speed and that there are no tissue structural changes such as coagulation because of the exposure to thermal dose (*i.e.*, similar tissue properties without **significant** changes in $\alpha(z)$ and $\beta(z)$). Eq. (10) shows that, potentially, the local temperature changes can be estimated directly by measuring local IF changes. Thus, the commonly used procedure that calculates displacement and then performs an axial derivative to obtain strain, *i.e.*, temperature changes, can be bypassed.

Numerical implementation of instantaneous frequency estimation

One common method for estimating the local IF is to measure zero crossings of the received radiofrequency (RF) signals (Boashash 1992a). For a sinusoidal signal under a fixed sampling rate, the signal can be considered to be locally stationary, and the frequency can be simply regarded as the inverse of the period or, alternatively, as half the inverse of the interval between the zero crossings $f_i\approx\frac{1}{2T_z}$, where T_z is the interval between two adjacent zero crossings if we assume that the zero crossings fall exactly on the sample points.

The advantage of using zero crossings to estimate the IF is that this method is computationally efficient. However, the disadvantage is that the frequency may not be optimized due to suboptimal conditions. Moreover, if the interval between the zero crossings is not an integer multiple of the samples, then quantization ''noise'' can be easily introduced in addition to linear averaging induced by the estimator. To reduce the variance in the zero-crossing-based IF estimation method, two approaches have been developed. First, we used the estimator proposed by O'Shea and Boashash, according to which the average number of zero crossings within a time series with adjacent 2 M points is taken as (O'Shea and Boashash 1990)

$$IF[n]\cong\frac{1}{2}\cdot\sum_{m=-M}^{M}|\mathrm{sgn}[s(m)]-\mathrm{sgn}[s(m-1)]|\cdot h(n-m), \quad (11)$$

where

$$\mathrm{sgn}[s(n)]=\begin{cases}1, & for\ s(n)\geq 0\\ -1, & for\ s(n)<0\end{cases}$$

and

$$h[n]=\begin{cases}1/2M, & for\ 0\leq n\leq M-1\\ 0, & otherwize\end{cases}.$$

The selection of M introduces a bias–variance tradeoff in the estimation. If M is large and the IF law is nonlinear within the processing window, a bias will be introduced. On the other hand, if M is small, the bias is likely to be reduced but at the cost of higher variance. In our application, to retain the spatial resolution of the estimated local temperature changes, we used a small processing window of approximately one cycle of the transmitted center frequency.

Implementation of IF-based temperature change estimation

In our implementation, eqn (9) is used instead of eqn (10) for temperature-change estimation because integration can smooth out the noise in the estimated IF caused by the discretized process and model errors, *i.e.*, the CW approximation used to derive eqn (6). In addition, a low-pass filter is used to further reduce the noise. In our method, the temperature change is estimated by the following equation, which has been modified from eqn (9):

$$\delta T(n) \approx k(n) \cdot [LPF\{AIF(n+1)\} - LPF\{AIF(n)\}], \quad (12)$$

where the constant term $C_0/2 \cdot (1/(\alpha(z)-\beta(z)))$ in Eq. (9) was represented as k(n). $LPF\{AIF(n)$ denotes the low-pass-filtered accumulated IF (AIF), which is calculated as follows:

$$AIF(n) = \sum_{k=1}^{n} (IF_2(k) - IF_1(k)). \quad (13)$$

Comparison with the standard cross-correlation algorithm

To evaluate the proposed IF-based processing scheme, a cross-correlation-based algorithm was implemented in this study based on a previously reported technology (Bonnefous and Pesque 1986; Maass-Moreno et al. 1996; Pernot et al. 2004). In the implementation of this algorithm, the time shift occurring between two consecutive RF A-lines is estimated by 1-D cross correlation. Processing window sizes of λ to 16λ were tested (λ represents the wavelength of the center frequency). This is equivalent to 40–640 data points after the interpolation of the used RF data, which is equivalent to a spatial resolution of 0.3–4.8 mm. All the filters used were identical to those used in the IF algorithm such that the comparison could be performed without variations induced by differing filters.

Experimental setup

Figure 1 shows the experimental setup of the system used in this study. A 1.5-MHz transducer was used to generate focused ultrasound exposure, which is made by 1–3 piezocomposite material, with a diameter of 6 cm and curvature radius of 8 cm (Imasonic, Besançon, France). A commercialized ultrasonic imager was used (Model T3000; Terason, Northborough, MA, USA), where its RF data could be obtained offline and postprocessed after the experiments. The imaging probe was a linear array with an operation frequency range of 5–12 MHz (the operating frequency was set at 5 MHz in this study). The beamformer system comprised 128 RF pulse-echo lines, with 4096 sample points in the B-mode sampled at the rate of 20 Msamples/s; each line can be transferred to the computer. Under this setting, ultrasonic imaging yielded a field of view with a depth of 40 mm and width of 38 mm. To monitor the maximum temperature change, the imaging planes were always positioned to allow one of the scanlines passing through the peak spot of focused ultrasound. The heating and imaging systems were interleaved with a cycle of 4 s (controlled by the computer), where the heating duration for the HIFU transducer was set at 3.5 s, with a B-mode data acquisition time of 0.5 s (the frame rate was approximately 0.25 Hz). To reduce the phase-wrapping problem, which may be induced when the temperature-induced echo time-shift exceeded the signal cycle, two consecutive imaging data were processed so that the temperature change between the two processed frames was minimal, thus reducing the occurrence of phase-wrapping.

The phantom or *ex vivo* tissue samples were diced to a depth of 6 cm, yielding a time-of-flight of approximately 80 μs with the sampling rate of 20 Msamples/s; this is equivalent to having four data points per signal cycle for signals with 5-MHz center frequency. To increase the number of data points (*i.e.*, increase the sampling rate),

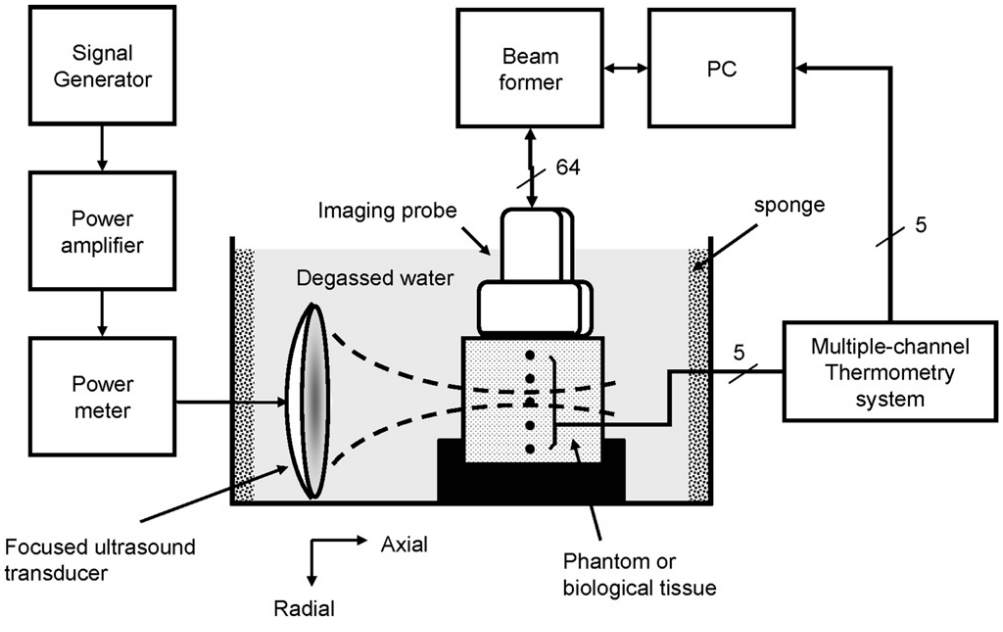

Fig. 1. Experimental setup.

a simple linear interpolation with a factor of 10 (a compromise between computational time and required resolution when estimating IF) was applied to yield 40 data points per cycle before processing under acceptable computational loading. The data after the interpolation can detect echo time-shift changes at 5 ns, which is equivalent theoretically to detecting a temperature change of 0.08°C because the maximum echo-time difference over the linear region (*i.e.*, 30 to 50°C) in Fig. 2 is 1250 ns. To reduce Gaussian noise in the imaging, a 2-D low-pass filter (2nd-order Butterworth filter implemented in frequency domain) was generally used. Because the IF was estimated from each RF signal cycle, a spatial resolution of 0.3 mm was obtained for temperature estimation before applying the low-pass filter theoretically. In addition, the low-pass filter used in eqn (13) is an 8-order finite-impulse-response filter with −6 dB cutoff frequency = 5.5 MHz.

Measurement of the speed of sound at different temperatures

Because the temperature-dependent changes in the speed of sound signify the main physical property used in the implementation of temperature estimation, the distribution of the sound speed was measured first before performing the heating experiment. To measure the sound speed for different heating temperatures, we used a time-of-flight sound speed measurement method under a transmission-type setup (Duck 1990; Lu et al. 1996). Two planar piezoelectric transducers (center frequency 3.5 MHz, diameter 10 mm, bandwidth 60%) were used and attached to the sample. The first one was used to generate a short burst pulse from one end, and the second one was used to receive the time-of-flight echo signal from the other end. A pulser-receiver (Model 5800PR; Panametrics, Inc., Waltham, MA, USA) was used to deliver the pulse to the transducer; the output signal was detected by an oscilloscope (Model 2014; Tektronix, Beaverton, OR, USA) and then sent to the PC *via* a general-purpose interface bus (GPIB) interface. A heating tank with temperature control ranging from 20–80°C was used as the uniform heating source for the testing samples. The testing samples included pure degassing water, tissue-mimicking graphite phantoms (Hynynen et al. 1983), and *ex vivo* porcine muscles. Thermocouples were both inserted into the samples and placed in water to monitor the temperatures. Data were collected until the temperature of the sample reached the setting temperature of the water in the heating tank. Then, the sound speeds at different controlled temperatures were calculated offline according to the received time-of-flight echo signals.

Temperature measurement

A multiple-channel thermocouple system was used to measure the temperature change to calibrate the estimated temperature. A bare-wire J-type thermocouple (O.D. = 0.2 mm per wire) was used to measure the phantom and tissue temperature; these data were fed back to the computer via an RS-232 interface. To minimize intervention in the temperature measurement of the axial direction (defined as the direction of the focused ultrasound transducer passing through the center of the hot spot, as illustrated in Fig. 1), only one temperature node was included. In the temperature measurement of the radial-direction (defined as the direction off the beam axis of the focused ultrasound transducer and along the beam direction of the imaging probe, as illustrated in Fig. 1), a maximum of five temperature nodes were included and spaced approximately 5 mm apart. (Because the dimension of the main lobe of the focal beam at the focal depth was approximately 2–3 mm, the outer thermocouples did not directly interfere with the wave.) The temperature information was output to the PC through the GPIB interface at a sampling rate of 0.25 s. Thermocouple insertion was simultaneously guided by a retaining needle (Hynynen et al. 1983) and ultrasound imager. To confirm the thermocouple tips being placed at the designated positions, pulsed-mode energy was delivered from the focused ultrasound applicator to stimulate the thermocouple. The transient temperature fluctuations were observed (typically less than 3°C) to find the focal position (*i.e.*, focal position always contains the maximum temperature).

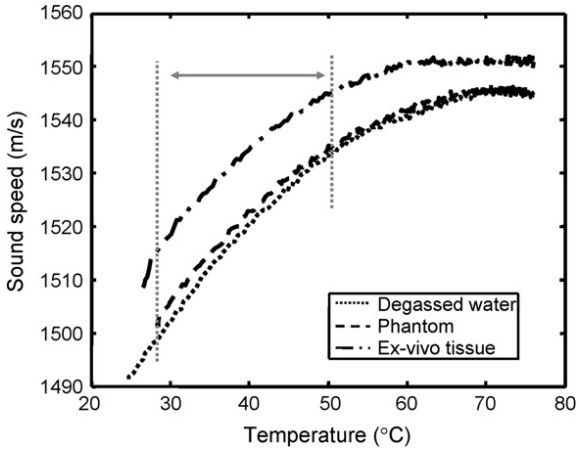

Fig. 2. Measured sound speed in different media at different temperatures. The different media include water, tissue-mimicking phantoms, and *ex vivo* porcine muscles. The two vertical dotted lines indicate a somewhat linear temperature-to-sound speed change region.

Evaluation of algorithm performance

To evaluate the performance of the proposed algorithm, the cross-correlation algorithm was used as the reference. The first index to be examined was the

computational efficiency of the algorithm. All data processing was performed using MATLAB (The MathWorks, Inc., Natick, MA, USA). To compare the processing speeds, both algorithms were tested in the same calculation environment (CPU: Intel Genuine T2300/1.66 GHz, Ram: 1 G Bytes/0.99 GHz; standard cross-correlation calculation provided by MATLAB was used, which is an optimized implementation for general-purpose applications. For estimating IF and temperature change, a custom-made algorithm implementing eqns (11) and (12) was used). The second index to be examined was the contrast-to-noise ratio (CNR) estimated from the temperature image, which has been used as a standard reference in quantifying the quality of strain imaging; it is given by (Varghese and Ophir 1998; Srinivasan et al. 2004)

$$CNR\ \ (in\ \ dB) = 20 \times \log_{10}\left(\frac{S_t - S_b}{\sigma_{S_t}^2 + \sigma_{S_b}^2}\right), \qquad (14)$$

where S_t and S_b denote the mean values of the temperatures within the target region and the background, respectively, and $\sigma_{S_t}^2$ and $\sigma_{S_b}^2$ denote the corresponding variances in these regions. The target and background regions were defined as pixels in the whole temperature image with the temperature-change value higher than 70% (at inner focal region) and lower than 50% (out of the focal region) of the peak value, respectively, and the image frame with the highest temperature was used. The third index to be examined was the axial resolution. The proposed algorithm detects the IF change cycle; therefore, the axial resolution equals approximately one wavelength of the RF signal (*i.e.*, 0.3 mm). In the cross-correlation algorithm, different axial resolutions are defined by the size of the segmented processing window. Different sizes of the processing windows were applied (ranging from 1λ to 16λ) to test the performance.

RESULTS

Figure 2 shows the temperature-induced changes in speed-of-sound changes in water, tissue-mimicking phantoms and porcine muscles. Monotonic changes in the sound speed can be measured for all the testing samples. The tissue-mimicking phantoms and water showed similar sound speed to temperature trends, whereas the porcine muscles exhibit higher sound speeds over the entire tested temperature range. Temperature-induced sound-speed changes were found to be somewhat linear only at temperatures lower than 65°C in the water/phantoms and 60°C in porcine muscles. This implies that the temperature estimation **simply by linear-scaling the echo time-shift** was limited below these threshold temperatures. A linear sound speed change ranging from 30–50°C was determined where the increase in the sound speed was approximately linear, and it was regarded as the temperature estimation region for the following experiments.

First, a comparison between the cross-correlation algorithm and the proposed algorithm was presented. The RF pulse-echo line crossing the focal position was analyzed. The power of the focused ultrasound was set to 30 W, and the heating time was 60 s. Tissue-mimicking phantoms were used in this section of the experiment. Figure 3a–3h show the accumulated echo time-shifts and their differentiations (analogous to temperature variation) from the conventional cross-correlation algorithm based on the implementation described in Maass-Moreno et al. (1996) and the proposed algorithm based on implementation from eqns (11)–(13). The test processing window was set, respectively, to 1λ, 4λ, 8λ and 16λ for the cases in (a), (c), (e) and (g) (before interpolation, the sampling points used per cycle were 6, 24, 48 and 96 points, which are equivalent to window sizes of 0.21, 0.84, 1.68 and 3.42 mm). For the data processed using the cross-correlation algorithm, the echo time-shift accumulation contains relatively high fluctuations when the processing window is small (*i.e.*, higher spatial resolution), whereas the curve estimated from a larger window size was smoother. This fluctuation can be filtered by the added low-pass filter mentioned above. When a larger processing window was used (*i.e.*, lower spatial resolution), a relatively unfiltered echo time-shift accumulation was obtained, but the trade-off is a decrease in the spatial resolution.

Figure 3i–3j show the results of implementation of the proposed IF-based algorithm. When we compared these processed results to those obtained from the cross-correlation algorithm, the echo time-shift signal before filtering still contained high-frequency fluctuations similar to the case where the cross-correlation estimation employed a small processing window. However, the filtered signal still seemed reasonably stable. The differentiated signal exhibits high specificity with regard to detection of the heat-up region. Further, for a window size equal to that used in the cross-correlation algorithm (shown in Fig. 3a and 3b)—*i.e.*, under the same spatial temperature estimation resolution—the temperature estimated by the cross-correlation algorithm contained relatively low noise in the inferior region off the image probe and behind the focal beam, but a more severe fluctuation than that in the IF estimation. On the other hand, a wider processing window in cross correlation resulted in smoother temperature estimation close to the heat-up region. However, the data shown in Fig. 3h that are inferior to the image probe were overestimated, and a significant amount of negative or positive noise was induced.

Figure 4 shows a comparison of computational efficiencies between the proposed algorithm and the

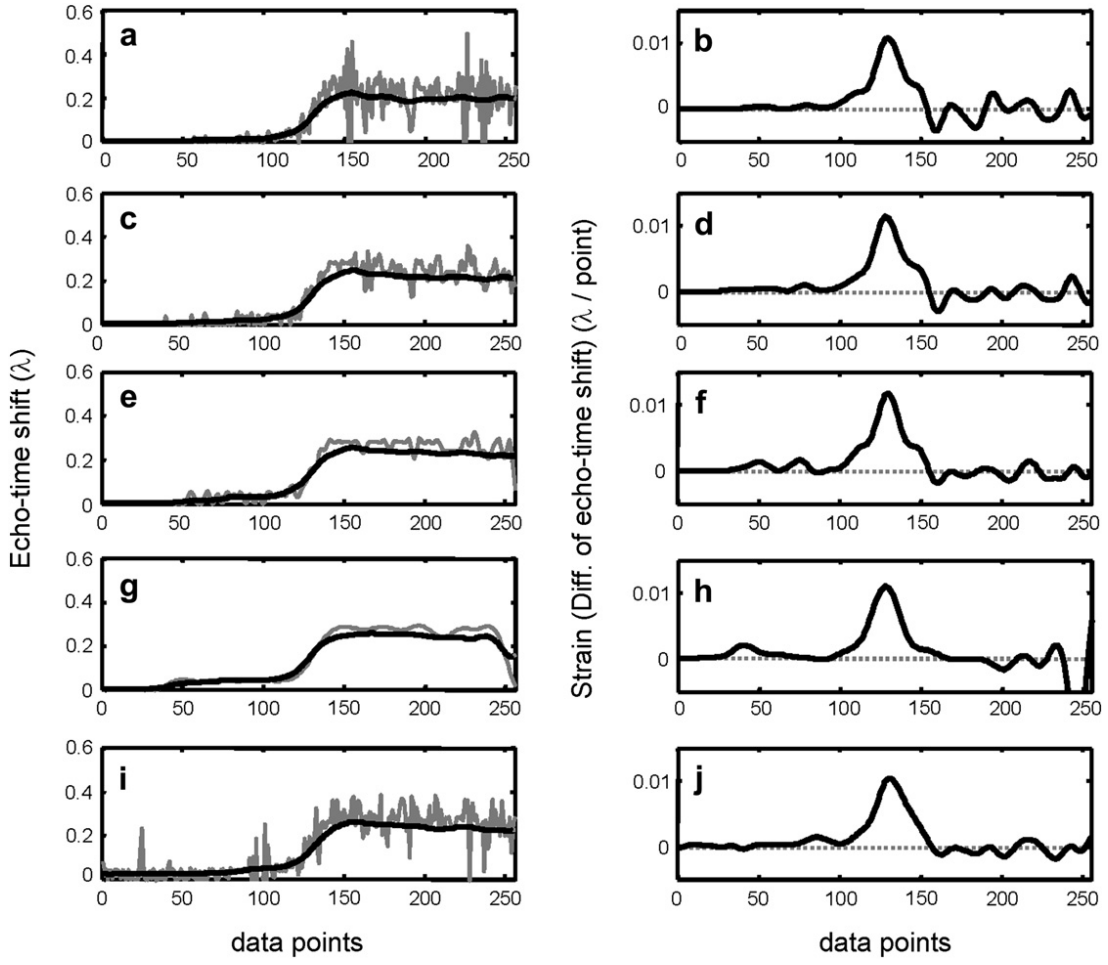

Fig. 3. Comparison of the echo time shift accumulation and its corresponding differentiation calculated from standard cross-correlation–based algorithms, shown in (a)–(h), and proposed instantaneous frequency-based algorithms, shown in (i) and (j). In the cross-correlation algorithm, different processing window sizes of 1, 4, 8 and 16 times the ultrasound signal cycle were used corresponding to the cases in (a), (c), (e) and (g), respectively.

cross-correlation-based temperature estimation algorithm (window sizes ranged from 1λ to 16λ). The results reveal that the IF algorithm had processing efficiency that was almost six times higher than that of the cross-correlation algorithm under the same resolution (*i.e.*, a processing window size of 1λ was used in cross-correlation algorithm). Increasing the processing window size in the cross-correlation algorithm can reduce the processing time because the total number of processing windows is reduced. However, no further reduction in the processing time was observed when increasing the processing window size greater than 6λ, and the IF-based algorithm still yielded a processing efficiency that was three times better than that obtained from the cross-correlation algorithm.

The CNR values obtained from these two algorithms were compared, and the results are shown in Fig. 5. In the cross-correlation algorithm, a small processing window size induced high fluctuations outside the heat-up region, and the CNR was relatively low. Processing window sizes ranging from 6–10λ yielded better noise rejection results than the proposed algorithm, and the CNR values could be increased by up to 37 dB. Longer processing window sizes did not provide further CNR improvements. In contrast, for the IF-based algorithm, the CNR value was superior (32 dB) when the processing window size used was the same as that in the cross-correlation algorithm with the smallest window size, *i.e.*, 1λ (CNR of approximately 25 dB). When the results shown in Figs. 4 and 5 are compared, it can be seen that the proposed algorithm yielded higher spatial resolution with superior processing efficiency, but the cross-correlation algorithm yielded superior noise rejection when the processing window size was optimized with a trade-off between lower spatial resolution and inferior processing efficiency.

Figure 6 shows the correlation between the IF-based temperature estimation (solid lines) compared with the measured values by thermocouples (dotted lines). Five thermocouples were placed diagonally to the RF

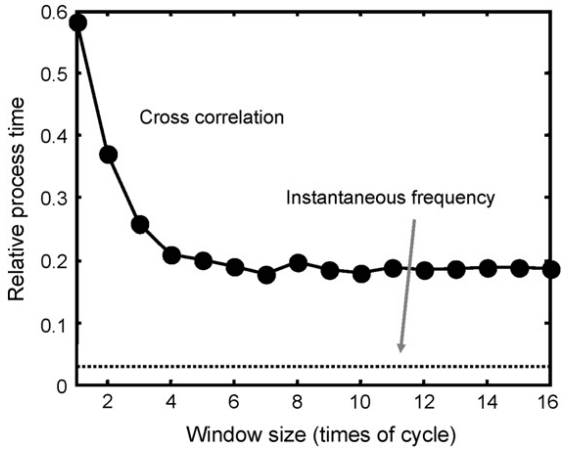

Fig. 4. Comparison of the relative processing efficiencies obtained from the cross-correlation algorithm employing different processing window sizes (ranging from 1 to 16 times the ultrasound signal cycle) and the proposed algorithm.

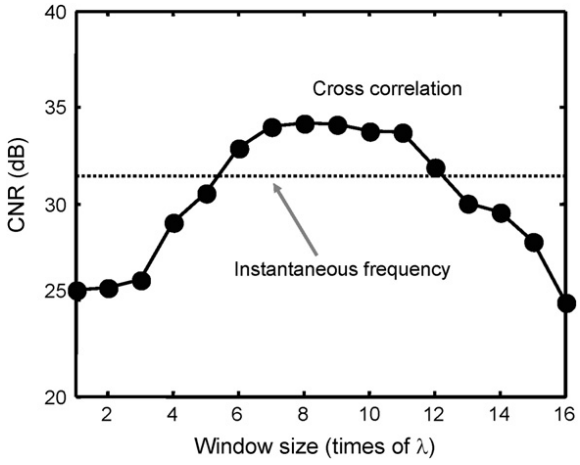

Fig. 5. Comparison of the signal-to-noise ratios obtained from the cross-correlation algorithm using different processing window sizes (ranging from 1 to 16 times the ultrasound signal cycle) and the proposed algorithm.

pulse-echo lines. In this setting, the A-line passing through the focus along the radial direction was used, and the tissue-mimicking phantoms were used for testing. An electrical power and sonication time of 50 W and 60 s were used, respectively. In this figure, only the data from the time points of 4, 12, 36 and 60 s are shown. The estimated echo time-shift was scaled to fit the measured temperature, and the scaling factor was fixed for later phantom or *ex vivo* tissue use. The results reveal that, after achieving adequate calibration, the estimated temperature elevation could have excellent correlation with the measured value. Further, it was revealed that good temperature prediction of up to 45°C at the peak temperature value could be obtained in tissue-mimicking phantoms.

Figure 7 shows the 2-D estimated temperature mapping of the tissue-mimicking phantoms. The orientation of the imaging probe was positioned such that the cross-sectional plane of the focal beam was imaged. The applied power was 30 W, and the heating duration was set to 40 s. For comparison, the maximum temperatures from the cross-correlation algorithm are shown in the top and middle panels (processing window sizes of 6λ and 16λ), and those from the proposed method are at the bottom. The maximum temperatures (denoted as T_{max}) estimated at different time points at 20, 40 and 80 s are shown, which represent the time points at the middle of heating, end of heating and the time after heating and during cooling, respectively. The maximum temperatures estimated from different algorithms were similar (difference within 1°C); here, after the power was turned off, the temperature gradually decreased to approach its base-line level (25°C). When these values are compared with the temperatures estimated from the cross-correlation algorithm using a small processing window ($\lambda = 6$) and those obtained from the proposed algorithm, the temperature estimation results were similar to either the peak temperature value or the noise level at shallow locations. However, the noise level was relatively high for the cross-correlation algorithm at deeper regions. The cross-correlation algorithm using a large processing window ($\lambda = 16$) appeared to have better noise rejection, as shown in Fig. 3. At the same time, unexpected, isolated high-level noise could be induced occasionally. A thermo-acoustic nonlinear effect was identified by the dark shadow artifact that occurred behind the heat-up region and existed in both implementations (Simon et al. 1998; Pernot et al. 2004). Further, for cross-correlation implementation with a long processing window (16λ), ringing noise patterns surrounding the heat-up region in this case could be observed. This artifact occurred when using an excessively long processing window in cross-correlation computation. This artifact became more apparent when using a longer processing window, and it degraded the CNR value when the processing window was larger than 10λ (see Fig. 5).

Figure 8 shows similar results, but the imaging probe was positioned along the axis of the focused ultrasound. No significant difference was found for the estimated temperatures between the cross-correlation–based algorithm and the proposed algorithm. The ringing-type artifact (as induced large negative or positive noise in Fig. 3h), as shown in Fig. 7, still occurred for the cross-correlation estimation using large processing window sizes.

In Fig. 9, the temperature evolution estimated from the cross-correlation algorithm and the proposed IF-based algorithm is shown along with the data acquired from the same experiment shown in Fig. 8. For the cross-correlation algorithm, the temperature evolution estimated with the

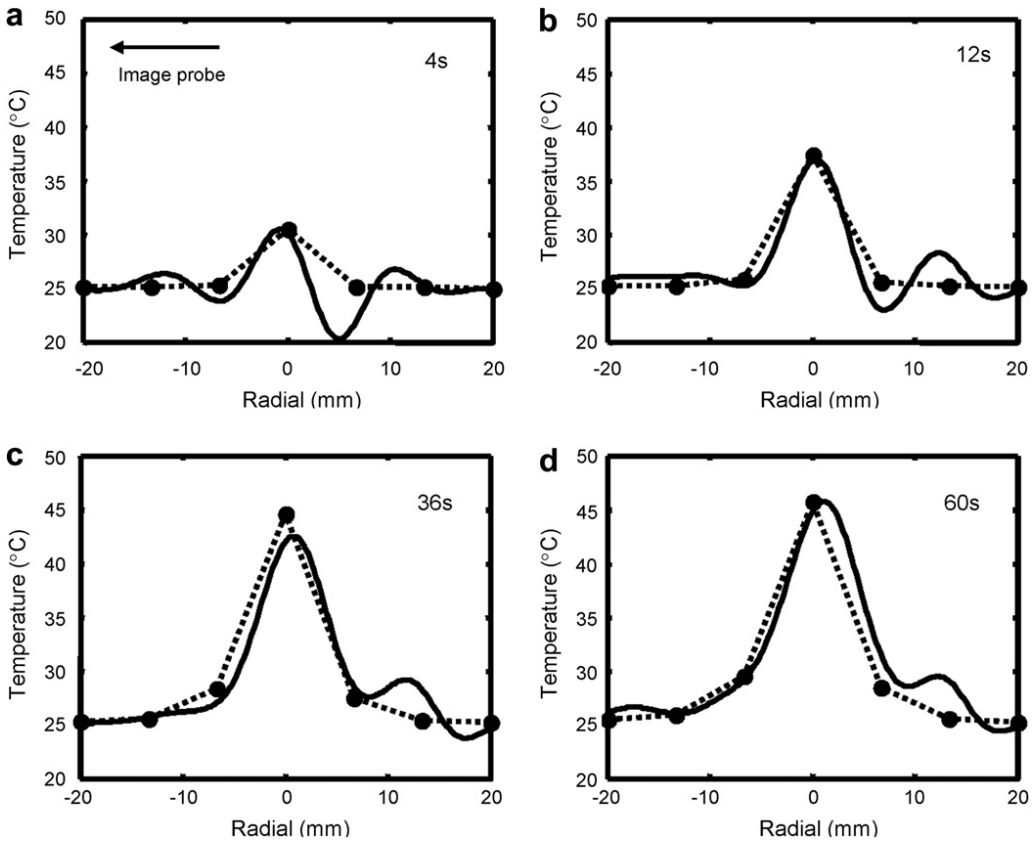

Fig. 6. Comparison of the measured temperature (*dotted lines*) and estimated temperature (*solid lines*) at different time points of the focused ultrasound sonication cycle. Electric power of 50 W was used to heat a tissue-mimicking phantom for a heating time of 60 s.

processing window $\lambda = 1$ is shown for simplicity (see Fig. 8a–c). Two sampled locations were selected for demonstration: (i) a region with an area of 1.5×1.5 mm^2 (approximately 10×10 pixels) was selected to show the temperature evolution close to the focal point (denoted as region 1); and (ii) the region posterior to the focal depth was selected (denoted as region 2). The temperatures estimated from both algorithms were similar with regard to temperature slopes, peak values and end points for these two selected regions. A larger discrepancy was observed at point 1 (focal position), particularly for the time period that contained large temperature gradients during the cooling phase.

Next we examined the temperature estimations from *ex vivo* porcine muscle experiments. The experimental setting was similar to the abovementioned tissue-mimicking phantom experiments. Two tissue sonications were performed. Tissue 1 was sonicated to generate a detectable but relatively small temperature change (<10°C) so that the tissue temperature could be well within the linear region for temperature estimation in our proposed technique, as indicated in Fig. 2. Tissue 2 was sonicated to produce thermal lesions with a large temperature increase (>20°C). The power delivered was set to 20 and 50 W in tissues 1 and 2, respectively, with the sonication durations both set to 80 s and an ultrasonic imaging sampling rate of 0.25 s. After the focused ultrasound power was turned off, additional ultrasonic images were acquired to observe the temperature reduction after heating. In tissue 1, one thermocouple was placed at the focal position to measure the peak temperature and compare it with the estimated temperature. Temperature maps estimated from tissue 1 and 2 sonications are shown in Figs. 10 and 11, respectively (both the original B-mode images and temperature distributions are shown at time points of 40 s, 80 s and 160 s). For both cases, the effects of temperature elevation cannot be directly observed from the original B-mode images, but the temperature can be quantified after applying the proposed algorithm. For tissue 1, one sample region (10×10 pixels) containing maximum temperature increase was selected (denoted as region 1); for tissue 2, we noted that one tissue interface existed on the main axis of focused ultrasound sonication, which can be identified from the produced hypoechos in B-mode images (denoted by the arrows in Figs. 11b and 11c) and the apparent temperature drop in the temperature maps, (denoted by the arrows in Figs. 11e and 11f). This interface caused a noticeable difference in temperature response between

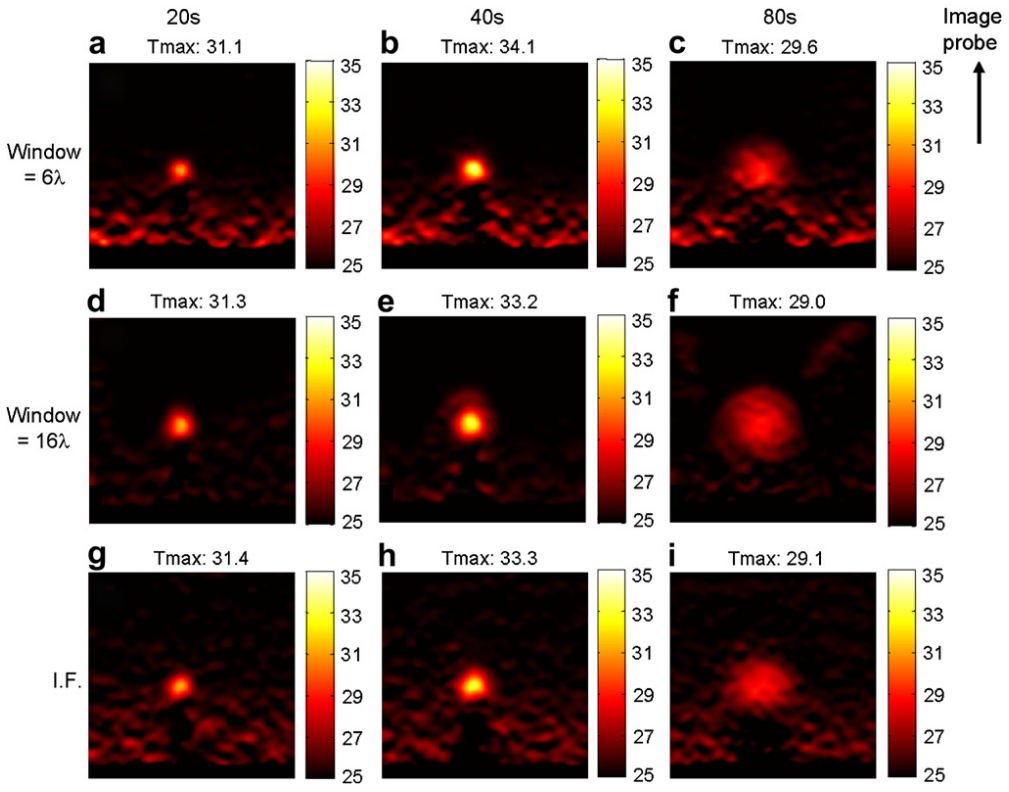

Fig. 7. Comparison of the estimated 2-D temperature distributions along the cross-sectional plane obtained from the cross-correlation algorithm (top and middle panels) and instantaneous frequency algorithm (bottom). Two processing window sizes of 1 and 16 times the ultrasound signal cycle are used in the cross-correlation algorithm. Electric power of 30 W was used to heat up a tissue-mimicking phantom for a heating time of 40 s. The temperature distributions at the time points of 20, 40 and 80 s are shown. All figures had dimensions of 40 × 40 mm.

the inferior and posterior location of this interface along the focused ultrasound axis indicated by the bottom-left arrow in Figs. 10 and 11. Hence, two sample regions were selected for demonstration (denoted as region 2 for the posterior one and region 3 for the inferior one).

Figure 12 shows the temperature evolutions of the three selected regions (mean plus one standard deviation within the regions was shown) of the *ex vivo* tissue experiments. The peak temperature was estimated to be about 33.7°C and 55.4°C in tissues 1 and 2, respectively. The estimated temperature of the selected region 1 in tissue 1 increased during the heating and decreased once the power was off and was found to well match the measured value by the thermocouple. In tissue 2, however, a temperature drop was observed in region 2 only but not in region 3 after the power was turned off.

The section of tissue 2 with sonication is shown in Fig. 13. The section of tissue 1 with sonication is not shown here because no thermal lesion was found. Observations of the coagulated regions confirmed that the heat-up regions from the temperature maps matched the coagulated regions, and one interface (denoted by the two white arrows) existing on the beam axis of the focused ultrasound also matched the locations of hypoechos and temperature drops observed in Fig. 11. Tissue coagulation was generated (confined to white regions) and located inferior to the interface. The temperature of this coagulated region (*i.e.*, region 3 in Figs. 11 and 13) exceeded 50°C (see Fig. 12) during the heating. The coagulation implies permanent tissue structure changes such as irreversible tissue expansion during the cool-down phase. Such tissue expansion during the cooling phase caused the insensitivity of our estimator to the temperature changes (Azuma et al. 2006) and thus resulted in the plateau of the region-3 curve in Fig. 12 after the power was off. In contrast, the region posterior to the interface—coinciding with region 2—did not show apparent tissue coagulation. Unlike region 3, the temperature response in region 2 appeared to decrease as expected when the power was turned off.

DISCUSSION

Phase-wrapping problem in the echo time-shift detection algorithm

The temperature-dependent speed of sound that results in echo time-shift was used in the proposed algorithm as well as the cross-correlation algorithm. To avoid the phase-wrapping problem, the basic assumption used is

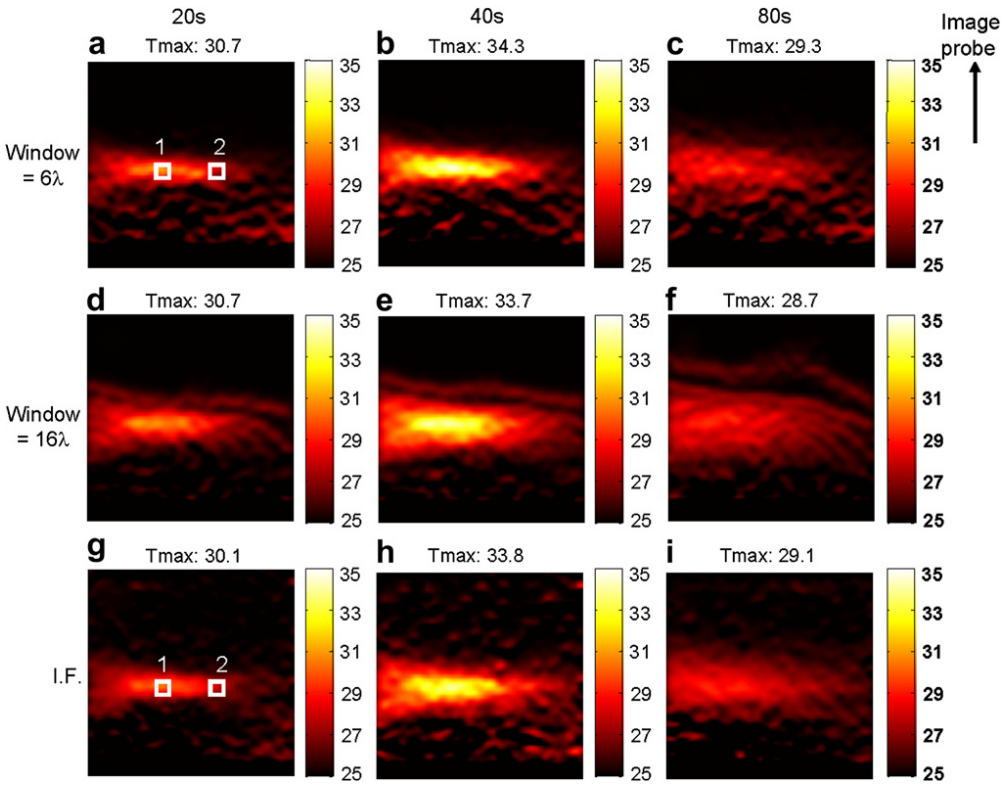

Fig. 8. Comparison of the estimated 2-D temperature distributions along the axial plane obtained from the cross-correlation algorithm (top and middle panels) and instantaneous frequency algorithm (bottom). Two processing window sizes of 1 and 16 times the ultrasound signal cycle are used in the cross-correlation algorithm. Electric power of 30 W was used to heat up a tissue-mimicking phantom for a heating time of 40 s. The temperature distributions at the time points of 20, 40 and 80 s are shown. All figures had dimensions of 40 × 40 mm.

that the echo time-shift distance induced by the temperature changes during the time period should not exceed one wavelength of the RF signal (Maass-Moreno and Damianou 1996; Maass-Moreno et al. 1996). In our experimental setup, a frequency of 5 MHz (*i.e.*, a period of 0.2 μs) was used for generating the RF pulse-echo signals, and the focus was generally located at a depth of 2 cm for a 4-cm-thick tissue or phantom. To avoid exceeding the 0.2-μs echo time-shift at the focal depth, the temperature change should be limited to within 10°C (calculated from Fig. 2). Similarly, to avoid the phase-wrapping problem in the entire 4-cm-long testing medium, the temperature change should be limited to within 5°C. Therefore, when increasing the temperature over 50°C to induce tissue coagulation, the phase-wrapping problem will occur if the temperature estimation at every time point always refers to the initial RF signals, thereby failing the temperature estimation. To minimize this effect, consecutive pairs of echoes were processed rather than processing all the echoes with respect to the initial one in our algorithm (Maass-Moreno et al. 1996); this approach effectively reduced the occurrence of the temperature elevation exceeding the phase-wrapping temperature threshold. Moreover, the RF-data sampling rate should be increased to reduce the temperature change levels between two adjacent times, thus reducing the phase-wrapping problem. Decreasing the diagnostic ultrasound frequency, which led to an increase in the wavelength

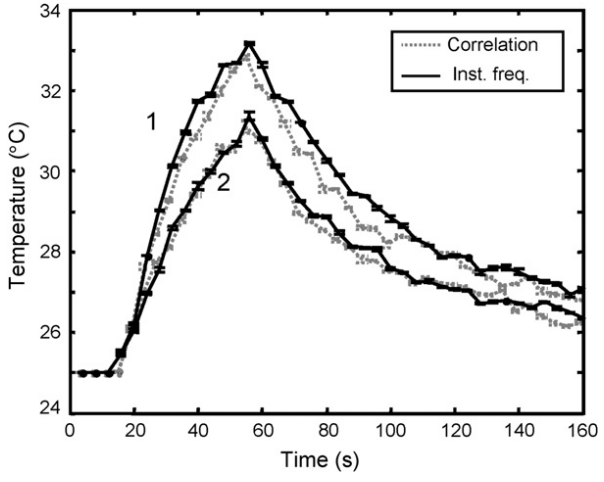

Fig. 9. Comparison of the temperature evolutions in two selected regions (denoted in Figs. 8a and 8g) obtained from the cross-correlation algorithm (*dotted lines*) and instantaneous frequency algorithm (*solid lines*).

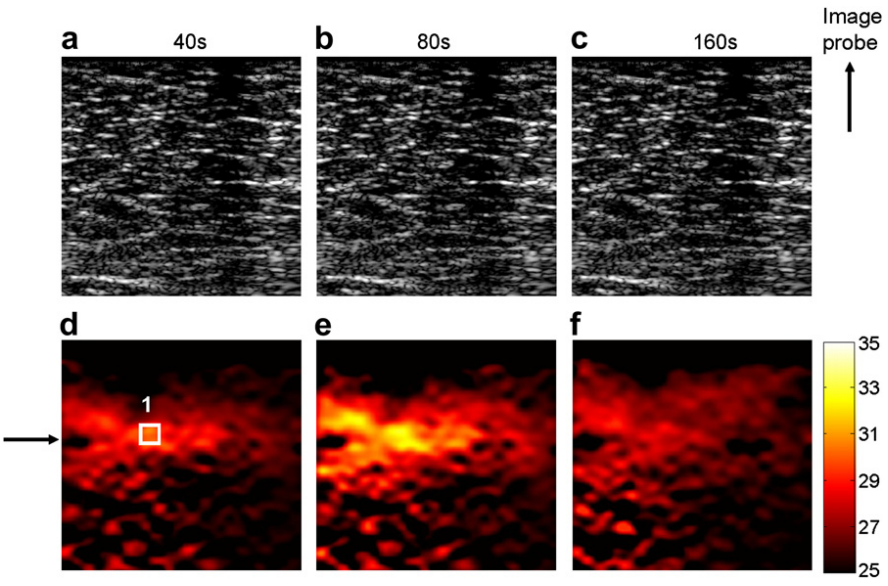

Fig. 10. B-mode images and temperature estimation of *ex vivo* tissue ablation (tissue sample 1). The applied power was 20 W for a heating time of 80 s. The imaging direction is parallel to the axis of the focused ultrasound. (a–c) B-mode images obtained at time points of 20 (in the middle of heating), 40 (at the end of heating) and 160 s (at the end of the overall session). (d–f) show the corresponding temperature mapping of (a)–(c). One region is marked as "1" in a later analysis of temperature response and examination of tissue sections. All figures had dimensions of 40 × 40 mm.

(resulting in a reduction in the imaging resolution), also yielded additional scope for temperature estimation without encountering the phase-wrapping problem. Other approaches such as unwrapping processing may be employed to solve the phase-wrapping problem (Bonnefous and Pesque 1986).

Difference between phantom and ex vivo *temperature estimation*

The temperature estimations from not only homogeneous phantoms but also biological tissues were confirmed by using the proposed algorithm. However, the temperatures estimated from the biological tissues contained higher fluctuations in the heat-up region (see Figs. 10 and 11) than those estimated from the homogeneous phantoms (see Figs. 7 and 8). Further, the temperature plateau of the temperature elevation obtained from phantom heating appeared to be more compact and uniform, and the temperature elevation in the *ex vivo* tissue appeared to be diverse, and it contained temperature variations. Some tissues also exhibited inhomogeneities or interfaces (denoted by white arrows), yielding higher impedance mismatches and causing lower ultrasonic energy transmission through them.

Limitation of this algorithm for temperature estimation

Simple temperature estimation relies on the consistent linear relationship between the sound speed and temperature such that consistent echo time-shift estimation can be obtained. The use of this hypothesis to monitor the heating of biological tissues, however, encounters practical obstacles. First, the relationship between sound speed change and temperature is not always linear. For muscles, a partial temperature range below 50°C was selected as a linear region and used to estimate the temperature by using constant scaling. When treating biological tissues at temperatures higher than 50 °C, the thermal dose accumulates rapidly and the tissues form permanent coagulation within a short duration, suggesting permanent tissue property changes, *e.g.*, permanent changes in speed of sound (Pernot et al. 2004) or irreversible tissue expansion (Azuma et al. 2006), and thus making echo time-shift insensitive to temperature changes. Therefore, obtaining accurate temperature estimates using an echo-time-shift-based approach over a coagulation threshold becomes more challenging because of this physical limitation. Using a fit to calibrate data that include the effects of permanent tissue property changes serves as one possible solution, with the trade-off of possible decrease in estimator SNR decrease when the temperature reaches the flat region of the curve and gained complexity in temperature calibration among different tissue types (Kaczkowski and Anand 2004).

Another limitation of our proposed approach is the narrow-band (or CW) approximation used to correlate the echo time-shift with IF in the derivation of eqns (9), (10) and (12). To perform temperature change estimation with eqn (12) accurately, narrow-band imaging pulses, *e.g.*, pulses with $<30\%$ fractional bandwidth as used in

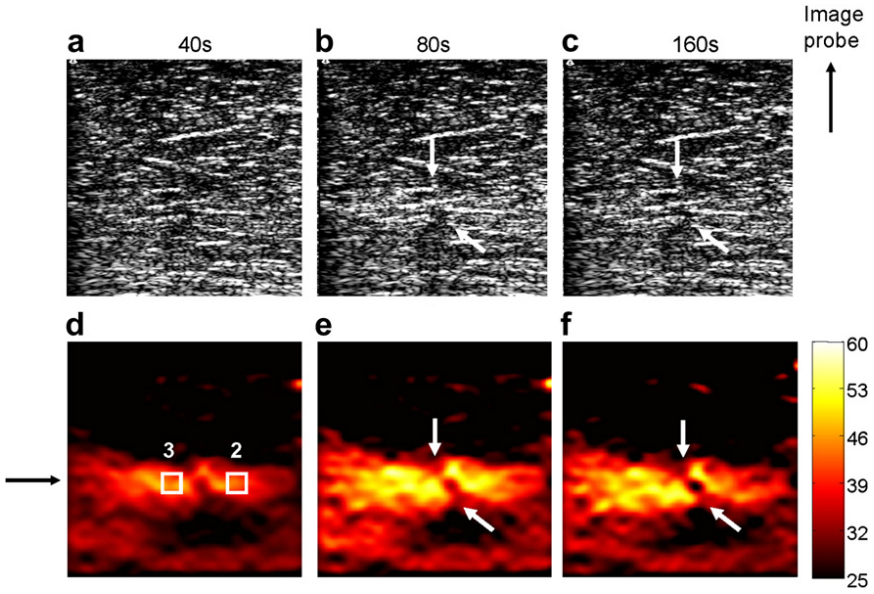

Fig. 11. B-mode images and temperature estimation of *ex vivo* tissue ablation (tissue sample 1). The applied power was 50 W for a heating time of 80 s. The imaging direction is parallel to the axis of the focused ultrasound. (a–c) show B-mode images obtained at time points of 40 (in the middle of heating), 80 (at the end of heating) and 160 s (at the end of the overall session). (d–f) show the corresponding temperature mapping of (a)–(c). Two regions are marked as "2" and "3," which are used in a later analysis of temperature response and examination of tissue sections. All figures had dimensions of 40 × 40 mm.

pulsed Doppler flow estimation, should be used. However, the clinical ultrasound imager used in the experiments employs wideband pulses for imaging (~50% fractional bandwidth with 5-MHz center frequency), which possibly prevented our direct implementation of temperature change estimation with eqn (10). Currently, we employ accumulated IF and low-pass filtering to reduce the noise (or error) in IF estimations (see eqn (12)). This compromise effectively reduced the noise level, and acceptable CNR could be obtained at the price of the degraded spatial resolution because of low-pass filtering. A potential approach to solving this problem could be applying narrow-band pass filtering to the received RF data before the temperature estimation, at the cost of lowering the spatial resolution.

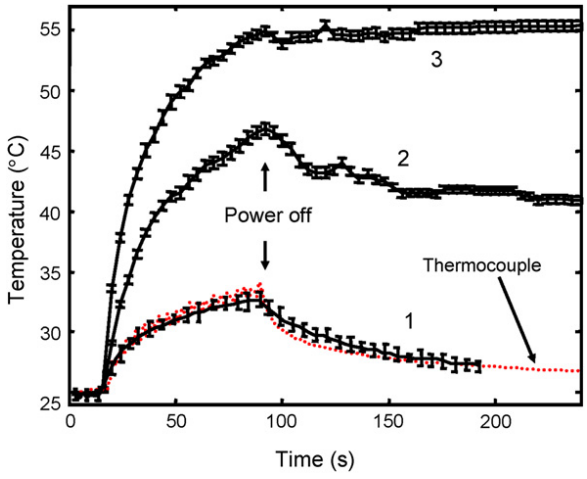

Fig 12. Temperature responses of the three selected regions from tissue 1 (region 1, indicated in Fig. 10d) and 2 (regions 2 and 3, indicated in Fig. 11d).

Aberration of temperature estimation in high-power thermal ablation

In the high-temperature *ex vivo* heating experiment, we observed that the estimated temperature in the coagulated tissue region did not truly reflect the actual temperature change. Tissue coagulation in region 3 in Fig. 13 implies permanent tissue property changes, which might cause permanent changes in speed of sound and irreversible tissue expansion. That is, such tissue expansion in coagulated regions remained unchanged during the cooling phase, which has been observed in M-mode images and reported by Azuma et al. (2006). Such unchanged tissue expansion in the cooling phase would cause our estimator to become insensitive to a decrease in temperature; thus possibly being one of the major causes of the plateau of the region-3 curve in Fig. 12 after the power was off. In addition, it was suspected that the thermal-acoustic nonlinear effect is another possible factor contributing to this artifact (Floch and Fink 1997; Simon et al. 1998; Hallaj et al. 2001; Pernot et al. 2004). Pernot et al. also provided evidence that when coagulation threshold reaches, thermal acoustic nonlinear effect due to permanent changes in speed of sound induces strong decorrelation on acquired RF signals, and extensively

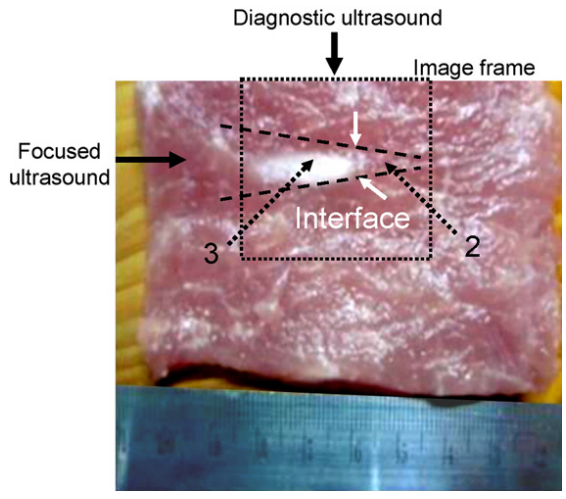

Fig. 13. *Ex vivo* muscle section of Fig. 11 (tissue 2). Note the tissue interface in the middle of the focused ultrasound beam (*white arrows*).

reduces the reliability of echo time-shift tracking (Pernot et al. 2002, 2004).

Instantaneous frequency detection implemented using zero-crossing technology

In this study, the performance of temperature estimation algorithms was based on the evaluation of computational efficiency, as opposed to noise level and spatial resolution. With regard to the evaluation of computational efficiency, our proposed algorithm was based on the detection of IF changes: this was implemented by using a zero-crossing technology to reduce the computational time. The implementation of zero crossings is extremely simple, and it is one of the most computationally efficient approaches for detecting IF. When used with ultrasound strain imaging, the higher computational efficiency of the zero-crossing approach has also been confirmed by another study (Srinivasan and Ophir 2003). Because of its simplicity, it is also an advantageous way of integrating the temperature-estimation function in current ultrasound imagers (up to six times faster than the standard cross-correlation algorithm used in our study).

On the other hand, the zero-crossing technology does not incorporate the optimal quadratic weighting function (Boashash 1992a) for IF detection. Another trade-off is that quantization noise is easily introduced if the interval between the zero crossings is not an integer multiple of the sampling points (Boashash 1992a). These factors contribute to a higher noise level in our implementation of IF detection and explain why the CNR values obtained from this algorithm are lower than those obtained from the optimized cross-correlation algorithm (approximately 5 to 8λ, see Fig. 5).

The other issue is spatial resolution. In our algorithm, zero crossings were tracked with a spatial resolution of approximately one wavelength; this does not require the segmentation of the RF A-line data into a specific processing window size, as carried out in the cross-correlation-based processing. This implies that, theoretically, the spatial resolution of the estimated temperature obtained from the proposed scheme is several times better than that obtained from the optimized cross-correlation algorithm (8 to 10λ) without the use of additional low-pass filters. Increasing the resolution in cross-correlation algorithms (*i.e.*, reducing the processed window size) degrades the CNR to a lower value than the values obtained from the proposed algorithm and simultaneously degrades the computational efficiency (see Figs. 4 and 5). Therefore, the IF-based algorithm has a greater potential to implement high-resolution temperature estimation intrinsically.

Sound speed measurement

The measured speed of ultrasound also coincided with results found in previous studies, which describe a monotonic increase of 20–50°C. However, some studies pointed out that, for temperatures greater than 55°C, the sound speed of tissue may be inversely proportional to temperature (Hallaj et al. 2001; Techavipoo et al. 2004). This phenomenon was not observed in our experiment, and two possible explanations were proposed. First, the selected tissue (porcine tenderloin muscle) differs from the tissue used in other studies to make this inverse transition not as apparent. Second, during sound-speed measurements, the water soaking into *ex vivo* tissues may introduce measured artifact in the high-temperature measurement case because a longer water-immersion duration was necessary when a higher target temperature was set (Hill 1986).

CONCLUSION

In this study, we propose a new approach for estimating temperature by using IF detection; it was implemented by using a simple zero-crossing algorithm. Some of the advantages of this approach are its superior computational efficiency and the possibility of achieving higher spatial resolution for temperature mapping. Further, the experimental results have demonstrated that the proposed algorithm possesses temperature-detection ability and precision that are comparable to the cross-correlation algorithm. Saturation of the estimated strain at temperatures greater than 50°C was observed, and the potential application of the proposed algorithm for thermal lesion detection was proposed. This study provides useful information as well as alternatives for the clinical applications of such an ultrasound-based temperature estimation technology.

Acknowledgement—This work was supported in part by National Science Council Grant No. 94-2262-E-182-008-CC3, Taiwan; National Health Research Institutes Grant No. 96A1-MEPP19-014, Taiwan; and the Chang-Gung Memorial Hospital Grant Nos. CMRPD34022, CMRPD34009, Linkou, Taiwan.

REFERENCES

Azuma T, Sasaki K, Kawabata K, Umemura S. Tissue expansion imaging for tissue coagulation mapping during high intensity focused ultrasound therapy. IEEE Ultrason Symp 2006;1770–1773.

Barber WD, Eberhard JW, Karr SG. A new time domain technique for velocity measurements using Doppler ultrasound. IEEE Trans Biomed Eng 1985;32:213–229.

Boashash B. Estimating and interpreting the instantaneous frequency of a signal—Part 2: Algorithms and applications. Proc IEEE 1992a;80: 540–568.

Boashash B. Estimating and interpreting the instantaneous frequency of a signal—Part 1: Fundamentals. Proc IEEE 1992b;80:520–538.

Bonnefous O, Pesque P. Time domain formulation of pulse-Doppler ultrasound and blood velocity estimation by cross correlation. Ultrason Imaging 1986;8:73–85.

Duck FA. Physical property of tissues—A comprehensive reference book. San Diego, CA: Academic Press; 1990.

Floch CL, Fink M. Ultrasonic mapping of temperature in hyperthermia: The thermal lens effect. IEEE Ultrason Symp 1997;2:1301–1304.

Hallaj IM, Cleveland RO, Hynynen K. Simulations of the thermo-acoustic lens effect during focused ultrasound surgery. J Acoust Soc Am 2001;109:2245–2253.

Hill CR. Physical principles of medical ultrasonics. Chichester. New York: E. Horwood, Halsted Press; 1986.

Hynynen K, Martin CJ, Watmough DJ, Mallard JR. Errors in temperature measurement by thermocouple probes during ultrasound induced hyperthermia. Br J Radiol 1983;56:969–970.

Kaczkowski PJ, Anand A. Temperature rise measured noninvasively during thermal therapy using backscattered ultrasound. Ultrason Symp 2004;1:720–723.

Kasai C, Namekawa K. Real-time two-dimensional blood flow imaging using an autocorrelation technieque. IEEE Ultrason Symp 1985;953–958.

Lu JL, Ying H, Sun ZG, Motamedi M, Bell B, Sheppard LC. In vitro measurement of speed of sound during coagulate tissue heating. IEEE Ultrason Symp 1996;1299–1302.

Lynn JG, Zwemer RL, Chick AJ, Miller AE. A new method for the generation and use of focused ultrasound in experimental biology. J Gen Physiol 1942;26:179–193.

Maass-Moreno R, Damianou CA. Noninvasive temperature estimation in tissue via ultrasound echo-shifts. Part I. Analytical model. J Acoust Soc Am 1996;100:2514–2521.

Maass-Moreno R, Damianou CA, Sanghvi NT. Noninvasive temperature estimation in tissue via ultrasound echo-shifts. Part II. In vitro study. J Acoust Soc Am 1996;100:2522–2530.

Nasoni R, Bowen T. Ultrasonic speed as a parameter for noninvasive thermometry. In: Mizushina S, (ed). Non-invsive Temperature Measurement. New York: Gordon and Breach; 1989. p. 95–107.

O'Shea P, Boashash B. Some robust instantaeous frequency estimation techniques with application to non-stationary transient detection. Proc EUSIPCO'90 1990;165–168.

Pernot M, Waters KR, Bercoff J, Tanter M, Fink M. Reduction of the thermo-acoustic lens effect during ultrasound-based temperature estimation. IEEE Ultrason Symp 2002;2. 1447–1150.

Pernot M, Tanter M, Bercoff J, Waters KR, Fink M. Temperature estimation using ultrasonic spatial compound imaging. IEEE Trans Ultrason Ferroelectr Freq Control 2004;51:606–615.

Rabinovici J, Inbar Y, Revel A, Zalel Y, Gomori JM, Itzchak Y, Schiff E, Yagel S. Clinical improvement and shrinkage of uterine fibroids after thermal ablation by magnetic resonance-guided focused ultrasound surgery. Ultrasound Obstet Gynecol 2007;30:771–777.

Seip R, Ebbini ES. Noninvasive estimation of tissue temperature response to heating fields using diagnostic ultrasound. IEEE Trans Biomed Eng 1995;42:828–839.

Simon C, Vanbaren P, Ebbini ES. Two-dimensional temperature estimation using diagnostic ultrasound. IEEE Trans Ultrason Ferroelectr Freq Control 1998;45:1088–1099.

Srinivasan S, Ophir J. A zero-crossing strain estimator for elastography. Ultrasound Med Biol 2003;29:227–238.

Srinivasan S, Ophir J, Alam SK. Theoretical derivation of SNR, CNR and spatial resolution for a local adaptive strain estimator for elastography. Ultrasound Med Biol 2004;30:1185–1197.

Stewart EA, Gostout B, Rabinovici J, Kim HS, Regan L, Tempany CM. Sustained relief of leiomyoma symptoms by using focused ultrasound surgery. Obstet Gynecol 2007;110:279–287.

Techavipoo U, Varghese T, Chen Q, Stiles TA, Zagzebski JA, Frank GR. Temperature dependence of ultrasonic propagation speed and attenuation in excised canine liver tissue measured using transmitted and reflected pulses. J Acoust Soc Am 2004;115:2859–2865.

Tempany CM, Stewart EA, McDannold N, Quade BJ, Jolesz FA, Hynynen K. MR imaging-guided focused ultrasound surgery of uterine leiomyomas: A feasibility study. Radiology 2003;226: 897–905.

ter Haar G. Ultrasound focal beam surgery. Ultrasound Med Biol 1995; 21:1089–1100.

ter Haar G, Coussios C. High intensity focused ultrasound: Physical principles and devices. Int J Hyperthermia 2007;23:89–104.

Varghese T, Ophir J. An analysis of elastographic contrast-to-noise ratio. Ultrasound Med Biol 1998;24:915–924.

Wu F, Wang ZB, Chen WZ, Zhu H, Bai J, Zou JZ, Li KQ, Jin CB, Xie FL, Su HB. Extracorporeal high intensity focused ultrasound ablation in the treatment of patients with large hepatocellular carcinoma. Ann Surg Oncol 2004;11:1061–1069.